1 Introduction

This document explains how our next**nano**py script 'Duboz2019.py' computes interband tunneling current through a highly-doped heterojunction. For the simulated structure and approximations, we refer to J-Y. Duboz and B. Vinter (2019) [1]. We first illustrate the formulation in Sec. 2, and then describe the algorithm implemented in the next**nano**py script in Sec. 3. Sec. 4 summarizes the prerequisites and different options in the script. Please refer to Table 1 for the notations.

Table 1: Summary of notation.

	growth direction	electrostatic potential
Doboz2019	z	V
this note	z	ϕ
next**nano**++	x	ϕ

2 6-band $\mathbf{k}\cdot\mathbf{p}$ Formulation

The 6-band $\mathbf{k}\cdot\mathbf{p}$ Hamiltonian consists of a perturbation quadratic in $\mathbf{k}$, spin-orbit splitting, crystal-field splitting, and strain Hamiltonian. Its eigenstates $|u_{vs}\rangle$ $(s = 1, \ldots, 6)$ are expressed in the basis $\{|X\rangle, |Y\rangle, |Z\rangle\} \otimes \{|\uparrow\rangle, |\downarrow\rangle\}$. The input file for next**nano**++ performs a self-consistent Schrödinger-Poisson calculation considering strain effects within the envelope function approximation to obtain the j-th eigenstate (eigenvalue E_{vj}) of the structure:

$$|\psi_{vj}\rangle = \sum_{\mu=1}^{3} [\alpha^j_{\mu\uparrow}\xi_{vj,\mu\uparrow}(z)|\mu\uparrow\rangle + \alpha^j_{\mu\downarrow}\xi_{vj,\mu\downarrow}(z)|\mu\downarrow\rangle], \tag{1}$$

where we label the orbital degrees of freedom by the index $\mu = X, Y, Z$, $\alpha^j_{\mu\sigma}$ and $\xi_{vj,\mu\sigma}$ are the spinor components and the valence band envelope functions of the j-th eigenstate, respectively. σ denotes the spin degrees of freedom. We model the conduction band states by the effective mass model for the Γ point. The i-th eigenstate (eigenvalue E_{ci}) is written as

$$|\psi_{ci\sigma}\rangle = \xi_{ci\sigma}(z)|S\sigma\rangle. \tag{2}$$

Matrix elements of the perturbation Hamiltonian (the elementary charge e [C] times the electrostatic potential ϕ [V]) for spin-conserving transitions

$j \to i$ are

$$
\begin{aligned}
M_{ij}^{\sigma} &= \sum_{\mu=1}^{3} \langle \mu\sigma | \xi_{vj,\mu\sigma}^{*} \alpha_{\mu\sigma}^{j*} \; e\phi \; \xi_{ci\sigma} | S\sigma \rangle \\
&\simeq c \sum_{R} \sum_{\mu=1}^{3} \alpha_{\mu\sigma}^{j*} \xi_{vj,\mu\sigma}^{*}(R) \xi_{ci\sigma}(R) \langle \mu\sigma | e \left[\phi(R) + \frac{\partial \phi}{\partial z}(R) z \right] | S\sigma \rangle \\
&\simeq c \sum_{R} \sum_{\mu=1}^{3} \alpha_{\mu\sigma}^{j*} \xi_{vj,\mu\sigma}^{*}(R) \xi_{ci\sigma}(R) e \frac{\partial \phi}{\partial z}(R) \langle \mu\sigma | z | S\sigma \rangle \\
&= c \sum_{R} \alpha_{Z\sigma}^{j*} \xi_{vj,Z\sigma}^{*}(R) \xi_{ci\sigma}(R) e \frac{\partial \phi}{\partial z}(R) \langle Z\sigma | z | S\sigma \rangle \\
&\simeq \alpha_{Z\sigma}^{j*} \int dz \; \xi_{vj,Z\sigma}^{*}(z) \xi_{ci\sigma}(z) e \frac{\partial \phi(z)}{\partial z} \langle Z\sigma | z | S\sigma \rangle,
\end{aligned} \tag{3}
$$

where c is the lattice constant in the growth direction and R labels the discrete unit cells. The electrostatic potential is assumed to be varying slowly in atomic lengthscales, but need not be constant over the tunneling region. The paper [Doboz2019], in contrast, approximates with a constant effective electric field. Only the Z components contribute to the transition because $\langle X|z|S\rangle = \langle Y|z|S\rangle = 0$. M_{ij}^{σ} has the unit [J]. For the envelope functions, we use the ones at $\mathbf{k}_{\parallel} = 0$. The Heisenberg equation for bare electrons under the unperturbed Hamiltonian translates the atomic matrix element as

$$
\begin{aligned}
\langle Z|p_z|S\rangle &= \langle Z| \frac{m_0}{i\hbar} [z, H_0] | S \rangle \\
&\simeq \frac{m_0}{i\hbar} (E_c - E_{v,\mathrm{av}}) \langle Z|z|S\rangle,
\end{aligned} \tag{4}
$$

where $E_{v,\mathrm{av}}$ is the eigenvalue of the unperturbed Hamiltonian in the absence of spin-orbit interactions. In the presence of spin-orbit interactions and crystal field (present in wurtzite crystals), $E_{v,\mathrm{av}}$ is shifted to heavy-hole (hh), light-hole, and split-off band energies:

$$
\begin{aligned}
E_{\mathrm{hh}} &= E_{v,\mathrm{av}} + E_A, \\
E_{\mathrm{lh}} &= E_{v,\mathrm{av}} + E_B,
\end{aligned} \tag{5}
$$

where the shifts are given by the splitting energies as (neglecting strain effect)

$$
\begin{aligned}
E_A &= \Delta_{\parallel} + \Delta_{\mathrm{cr}}, \\
E_B &= \frac{\Delta_{\mathrm{cr}} - \Delta_{\parallel}}{2} + \sqrt{\left(\frac{\Delta_{\mathrm{cr}} - \Delta_{\parallel}}{2} \right)^2 + 2\Delta_{\perp}^2}.
\end{aligned} \tag{6}
$$

For GaN, for instance, $E_A = 16$ and $E_B = 12$ meV. The next**nano**++ output of 'bandgap.dat' > 'Bandgap_Gamma [eV]' gives the gap between the gamma band and the highest valence band. For the present system, the highest valence band is the light-hole, i.e. next**nano**++ output is $E_c - E_{\rm lh}$. We thus calculate the bandgap in Eq. (4) by

$$E_g \equiv E_c - E_{v,\rm av} = E_c - E_{\rm lh} + E_B. \tag{7}$$

next**nano**py converts the unit from [eV] to [J]. Since the Kane parameter for the wurtzite crystal is related to the momentum matrix element by $P_1 = -\frac{i\hbar}{m_0}\langle S|p_z|Z\rangle = \frac{i\hbar}{m_0}\langle Z|p_z|S\rangle$, Eq. (4) becomes

$$\langle Z|z|S\rangle = \frac{1}{E_g}\frac{i\hbar}{m_0}\langle Z|p_z|S\rangle = \frac{P_1}{E_g}. \tag{8}$$

Note that in Eq. (4), $\langle Z|z|S\rangle$ is real while $\langle Z|p_z|S\rangle$ is pure imaginary. next**nano**++ prints out P_1 in the unit of [eV Å], which next**nano**py translates to [J nm], so that the dipolar moment (8) is in [nm]. Eqs. (3) and (8) lead to

$$M_{ij}^{\sigma} = \alpha_{Z\sigma}^{j*}\int \frac{P_1}{E_g}\xi_{vj,z\sigma}^{*}(z)\xi_{ci\sigma}(z)e\frac{\partial\phi(z)}{\partial z}dz, \tag{9}$$

where the coordinate z is in [nm] in next**nano**++, resulting in M_{ij}^{σ} [J]. The tunnel current due to a transition $j \to i$ is calculated from Fermi's golden rule as

$$\begin{aligned} I_{ij}\cdot L_xL_y &= e\cdot(\text{transition probability } j\to i) \\ &= e\sum_{\sigma}\sum_{\mathbf{k}_{c\parallel}}\sum_{\mathbf{k}_{v\parallel}}\frac{2\pi}{\hbar}|M_{ij}^{\sigma}|^2\delta\left(E_{vj} - \frac{\hbar^2k_{v\parallel}^2}{2m_v} - E_{ci} - \frac{\hbar^2k_{c\parallel}^2}{2m_c}\right), \end{aligned} \tag{10}$$

where I_{ij} is the current density, L_xL_y is the area of the plane and $\mathbf{k}_{c,v\parallel}$ are the in-plane wave vector of the electrons and holes, respectively. Here, the bandstructure is assumed to be parabollic. The occupation factors are taken to be 1 in the valence band and 0 in the conduction band.

[Duboz2019] focuses on the case where the in-plane momentum is conserved during the transition: $\mathbf{k}_{c\parallel} = \mathbf{k}_{v\parallel}$. The joint density of states without spin degeneracy

$$\begin{aligned} \rho_{ij} &\equiv \sum_{\mathbf{k}_{\parallel}}\delta\left(E_{vj} - E_{ci} - \frac{\hbar^2k_{\parallel}^2}{2m_v} - \frac{\hbar^2k_{\parallel}^2}{2m_c}\right) \\ &= \sum_{\mathbf{k}_{\parallel}}\delta\left(E_{vj} - E_{ci} - \frac{\hbar^2k_{\parallel}^2}{2m_r}\right), \end{aligned} \tag{11}$$

is given by the reduced mass: $1/m_r = 1/m_c + 1/m_v$. Assuming the heterostructure to be large in the in-plane directions, we turn the sum into an integral:

$$\rho_{ij} = \frac{1}{(2\pi/L_x)(2\pi/L_y)} \int dk_x \int dk_y \delta \left(E_{vj} - E_{ci} - \frac{\hbar^2 k_\parallel^2}{2m_r} \right), \tag{12}$$

where $k_\parallel^2 = k_x^2 + k_y^2$. We then switch to the polar coordinates by $k_x = k_\parallel \cos\theta, k_y = k_\parallel \sin\theta$, and $dk_x dk_y = k_\parallel dk_\parallel d\theta$:

$$\begin{aligned} \rho_{ij} &= \frac{L_x L_y}{(2\pi)^2} \int_0^{2\pi} d\theta \int_0^\infty k_\parallel dk_\parallel \delta \left(E_{vj} - E_{ci} - \frac{\hbar^2 k_\parallel^2}{2m_r} \right) \\ &= \frac{L_x L_y}{2\pi} \int_0^\infty k_\parallel \delta \left(E_{vj} - E_{ci} - \frac{\hbar^2 k_\parallel^2}{2m_r} \right) dk_\parallel. \end{aligned} \tag{13}$$

Changing the variables from $k_\parallel$ to $\varepsilon = \hbar^2 k_\parallel^2/(2m_r)$ yields

$$\begin{aligned} \frac{\rho_{ij}}{L_x L_y} &= \frac{1}{2\pi} \int_0^\infty \delta \left(E_{vj} - E_{ci} - \varepsilon \right) \frac{m_r}{\hbar^2} d\varepsilon \\ &= \begin{cases} \dfrac{m_r}{2\pi\hbar^2} & (E_{vj} > E_{ci}) \\ 0 & (\text{otherwise}) \end{cases} \end{aligned} \tag{14}$$

Eqs. (10) and (14) lead to the tunnel current density [A/m^2] for the case $E_{vj} > E_{ci}$:

$$I_{ij} = \frac{2\pi e}{\hbar} \sum_\sigma |M_{ij}^\sigma|^2 \cdot \frac{m_r}{2\pi\hbar^2} = \frac{e m_r}{\hbar^3} \sum_\sigma |M_{ij}^\sigma|^2, \tag{15}$$

where

$$|M_{ij}^\sigma|^2 = |\alpha_{Z\sigma}^j|^2 \left| \int \frac{P_1}{E_g} \xi_{vj,z\sigma}^*(z) \xi_{ci\sigma}(z) e \frac{\partial \phi(z)}{\partial z} dz \right|^2. \tag{16}$$

Total current for a given bias is

$$I = \sum_{E_{vj} > E_{ci}} I_{ij}. \tag{17}$$

3 What does the nextnanopy?

The next**nano**py script

1. runs the next**nano**++ simulations based on user-defined parameters
2. loads from the next**nano**++ output the envelopes $\xi_{vj,z1}, \xi_{vj,z2}$, and ξ_{ci} [nm$^{-1/2}$] and electrostatic potential $\phi(z)$ [V] as a function of position

3. differentiates the potential
4. reads in the position-dependent material parameters, calculates dipole matrix elements (8) and plots them as a function of position
5. perform the integration in Eq. (9)
6. computes Eq. (15) and translates to the unit [A/cm^2]
7. takes the sum (17)
8. sweeps the bias and repeats 2-7 above
9. exports the bias dependence of the tunnel current in the following formats:
    - 'Plots' tab within Spyder
    - image file with the format specified in the next**nano**py script
    - .dat file

    The latter two are stored in the folder indicated right before the end of the console log. .dat file is useful if you compare different I-V curves using next**nano**mat overlay.

4 Further remarks on the simulation

- The junction is pseudomorphically grown on $Al_{0.4}Ga_{0.6}N$ (previous version assumed GaN substrate).
- The temperature affects the bandgap and Fermi-Dirac distribution function. To comply with Duboz2019 (fully-occupied valence band and empy conduction band), we choose 4 K to suppress thermal excitations.
- If the bool variable 'CalculateEffectiveField_fromOutput' is set to 'True', next**nano**py calculates the position-dependent effective field in Eq. (9) from the electrostatic potential in the next**nano** output. When 'False', the assuption in the paper $\partial\phi/(\partial z) = 1$ [V/nm] is used. Default: True.
- If the bool variable 'KaneParameter_fromOutput' is set to 'True', next**nano**py reads in the Kane parameter P_1 in Eq. (8) from the next**nano**++ output. In this case, an 8-band $\mathbf{k}\cdot\mathbf{p}$ simulation with exactly the same device geometry will be performed so that next**nano**py can extract the Kane parameter. If 'False', P_1 is calculated from the assumption in the paper (E_{P1} =15 eV). Default: True.

- If the bool variable 'CalculateReducedMass_fromOutput' is set to 'True', next**nano**py calculates the position-dependent reduced mass in Eq. (15) using the next**nano** output of the split-off- and Γ band effective masses. When 'False', the assuption in the paper $m_r = 0.18m_0$ is used. Default: False.

- For reference, the sum of the envelope overlap squared

$$\sum_{j>i} \left| \int \xi^*_{vj,z\sigma}(z)\xi_{ci\sigma}(z)dz \right|^2 \tag{18}$$

  is calculated and printed in the console output. This quantity is not used in the tunnel current calculation as we compute the integral (9) instead.

- Duboz *et al.* simulated with single-band models for the valence band. While the 6-band $\mathbf{k}\cdot\mathbf{p}$ model makes more sense to evaluate valence band eigenstates in heterostructures, we implemented an option in the next**nano**py script. If you set 'Run_KP6 = False' and 'Run_SingleBand = True', Eq. (9) is computed with the effective mass model for the split-off band. Please refer to Sec. 5 for the formulation.

5 Single-band Formulation

The single-band Hamiltonian consists of an effective-mass Hamiltonian and strain Hamiltonian. We consider the Γ-band for electrons and HH, LH, and SO bands for holes. The next**nano**++ simulation yields eigenstates of the structure:

$$\begin{aligned}
|\psi_{c,i}\rangle &= \xi_{c,i}(z)|S\rangle, \\
|\psi_{\mathrm{HH},j}\rangle &= \xi_{\mathrm{HH},j}(z)|u_{\mathrm{HH}}\rangle, \\
|\psi_{\mathrm{LH},j}\rangle &= \xi_{\mathrm{LH},j}(z)|u_{\mathrm{LH}}\rangle, \\
|\psi_{\mathrm{SO},j}\rangle &= \xi_{\mathrm{SO},j}(z)|u_{\mathrm{SO}}\rangle,
\end{aligned}$$

where $\xi_{,j}$ are the envelope functions of the j-th eigenstate. In the single-band model spin states are degenerate. The matrix element of the perturbation Hamiltonian for a transition $j \to i$ is

$$\begin{aligned}
M^{\mathrm{SO}}_{ij} &= \langle u_{\mathrm{SO}}|\xi^*_{\mathrm{SO}j}\ e\phi\ \xi_{ci}|S\rangle \\
&\simeq c\sum_R \xi^*_{\mathrm{SO},j}(R)\xi_{ci}(R)\langle u_{\mathrm{SO}}|e\left[\phi(R) + \frac{\partial\phi}{\partial z}(R)z\right]|S\rangle \\
&\simeq c\sum_R \xi^*_{\mathrm{SO},j}(R)\xi_{ci}(R)e\frac{\partial\phi}{\partial z}(R)\langle u_{\mathrm{SO}}|z|S\rangle \\
&\simeq \int dz\ \xi^*_{\mathrm{SO},j}(z)\xi_{ci}(z)e\frac{\partial\phi(z)}{\partial z}\langle u_{\mathrm{SO}}|z|S\rangle,
\end{aligned} \tag{19}$$

and similarly for the transitions between the conduction band and HH or LH states. Using Eqs. (11)-(13) of [Duboz2019] and (8) above, we obtain

$$\begin{aligned}
\langle u_{\mathrm{HH}}|z|S\rangle &= 0, \\
\langle u_{\mathrm{LH}}|z|S\rangle &= \beta\langle Z|z|S\rangle = \beta\frac{P_1}{E_g}, \\
\langle u_{\mathrm{SO}}|z|S\rangle &= \beta'\langle Z|z|S\rangle = \beta'\frac{P_1}{E_g},
\end{aligned}$$

where the coefficients β and β' depends in principle on alloy content and strain. For the present structure the envelope overlap with the conduction band is much larger for SO than HH and LH states, which allows us to neglect the contributions from the latter two. We use an analytical formula for β' derived for unstrained bulk wurtzite [2]:

$$\beta'^2 = \frac{E_B^2}{E_B^2 + 2\Delta_3^2}, \tag{20}$$

where E_B is defined in Eq. (6) and material parameters depend on position z. Eq. (19) then becomes [compare with Eq. (9)]

$$M_{ij}^{\mathrm{SO}} = \int \beta'\frac{P_1}{E_g}\xi_{\mathrm{SO},j}^*(z)\xi_{ci}(z)e\frac{\partial\phi(z)}{\partial z}dz, \tag{21}$$

The tunnel current density due to a transition $j \to i$ is nonzero if $E_{vj} > E_{ci}$ and reads

$$\begin{aligned}
I_{ij}\cdot L_x L_y &= e\sum_{\mathbf{k}_{c\parallel}}\sum_{\mathbf{k}_{v\parallel}}\frac{2\pi}{\hbar}|M_{ij}^{\mathrm{SO}}|^2\delta\left(E_{vj} - \frac{\hbar^2 k_{v\parallel}^2}{2m_v} - E_{ci} - \frac{\hbar^2 k_{c\parallel}^2}{2m_c}\right), \\
I_{ij} &= \frac{2\pi e}{\hbar}|M_{ij}^{\mathrm{SO}}|^2\cdot\frac{m_r}{2\pi\hbar^2} \\
&= \frac{em_r}{\hbar^3}|M_{ij}^{\mathrm{SO}}|^2
\end{aligned} \tag{22}$$

where

$$|M_{ij}^{\mathrm{SO}}|^2 = \left|\int \beta'\frac{P_1}{E_g}\xi_{\mathrm{SO},j}^*(z)\xi_{ci}(z)e\frac{\partial\phi(z)}{\partial z}dz\right|^2. \tag{23}$$

Total current for a given bias is given by Eq. (17). The results from (i) 6-band $\mathbf{k}\cdot\mathbf{p}$ simulation and (ii) single-band model are shown in Fig. 1.

References

[1] Jean-Yves Duboz and Borge Vinter. Theoretical estimation of tunnel currents in hetero-junctions: The special case of nitride tunnel junctions. *J. Appl. Phys.*, 126:174501, 2019.

[2] S. L. Chuang and C. S. Chang. k·p method for strained wurtzite semiconductors. *Phys. Rev. B*, 54:2491–2504, Jul 1996.

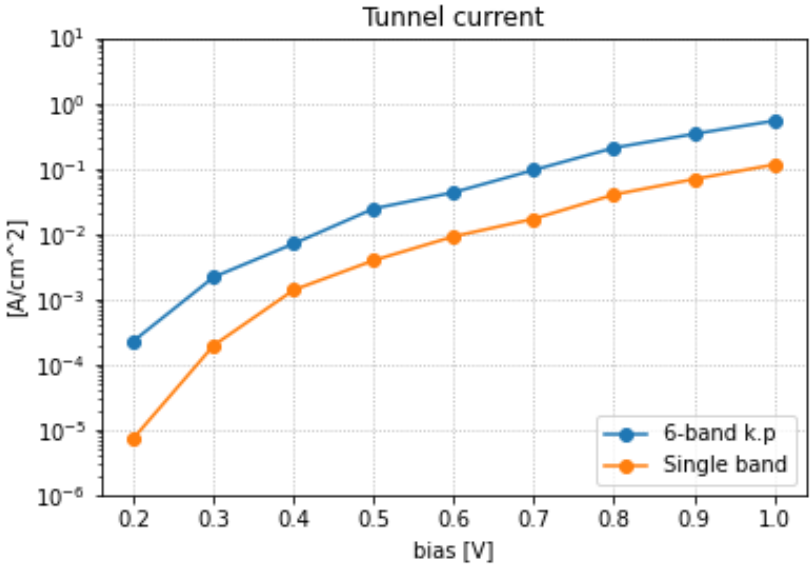

Figure 1: Simulation results of the 6-band $\mathbf{k} \cdot \mathbf{p}$ and single-band models. Effective fields and the Kane parameter are calculated from next**nano** output, while the reduced mass is taken from Ref. [1].